2025 IEEE/RSJ International Conference on Intelligent Robots and Systems (IROS 2025)
October 19-25, 2025. Hangzhou, China

2025 IEEE/RSJ International Conference on Intelligent Robots and Systems (IROS) | 979-8-3315-4393-8/25/$31.00 ©2025 IEEE | DOI: 10.1109/IROS60139.2025.11247220

ASV-Aided AUV Navigation: A Field Study on Nonlinear Estimation for Localization of Low-Cost, Scalable Systems

Raymond Turrisi[1,2], Daniel A Duecker[1,3], John Morrison[1,2], Fabian Steinmetz[4], Michael Benjamin[1]

***Abstract*— This work investigates the use of multiple Autonomous Surface Vehicles (ASVs) as Communication/Navigation Aids (CNAs) to enhance the navigation and state estimation of an Autonomous Underwater Vehicle (AUV). Our approach builds on recent advancements in low-cost sensors and platforms, which enable novel AUV applications across fundamental science, commercial industries, and defense. We consider six different combinations of Kalman Filter and Factor Graph localization solutions on three datasets, covering 53 minutes and 3.1 kilometers of operation. We first present the solution using the measurements from all three ASVs, before occluding measurements from two of the ASVs to assess the effect of reduced observability on localization performance.**

I. Introduction

A. Overview

Accurate navigation is a core challenge for Autonomous Underwater Vehicles (AUVs), which cannot use a Global Navigation Satellite System (GNSS) or RF signals while submerged. The key difficulty lies in estimating lateral (X-Y) positioning, as low cost ($< \$10,000$) heading and speed sensors are highly susceptible to drift. Magnetic compasses report heading errors between 0.5° and 2° in ideal conditions, but often perform worse in practice. Speed estimation further complicates the problem, as Doppler Velocity Logs (DVLs) require a seafloor reference (achieved at a low altitude) and may be unavailable in deep water missions. As a result, heading and velocity errors can cause dead reckoning estimates to drift tens to hundreds of meters during a 1 kilometer mission. While surfacing to obtain a GPS fix is an option, it is often impractical during extended field deployments.

In our approach, we propose using Autonomous Surface Vehicles (ASVs) as mobile navigation aids to an AUV in operation. Each ASV can access GNSS and maintain high-bandwidth communication links, while transmitting its position via low-cost acoustic modems to the submerged AUV. By measuring Two-Way-Travel Time (TWTT) between the AUV and ASV, we can constrain AUV navigation drift in real time without fixed beacons or frequent surfacing.

[1]Department of Mechanical Engineering, Massachusetts Institute of Technology, Cambridge, MA 02139, USA.
[2]Woods Hole Oceanographic Institution, Woods Hole, MA 02543, USA.
[3] Munich Institute of Robotics and Machine Intelligence (MIRMI) - Technical University of Munich (TUM), 80992 Munich, Germany.
[4] Institute for Autonomous Cyber-Physical Systems, Hamburg University of Technology (TUHH), 21073 Hamburg, Germany.
Corresponding author: rturrisi@mit.edu.
This work was supported by the National Defense Science and Engineering Graduate (NDSEG) Fellowship Program.
The authors would like to thank the Bavarian State Ministry for Science and the Arts (StMWK) for partial support as part of the project MITxTUM Alliance (grant number: 151223031).

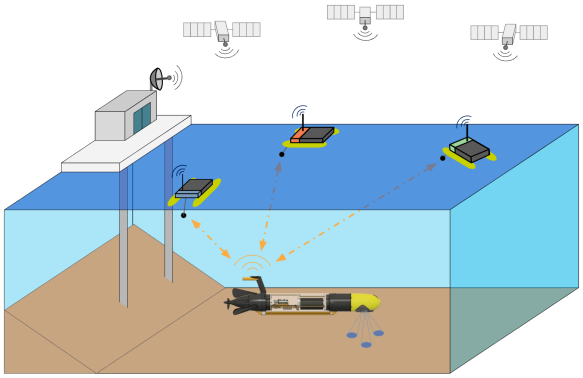

Fig. 1: A high-level illustration for the systems tested in this paper: Three ASVs with access to GNSS relay position updates to a submerged AUV using acoustic communications.

We investigate multiple nonlinear filtering strategies to fuse AUV dead reckoning sensors (DVL, AHRS, and depth) with acoustic-range measurements from one or more ASVs. We consider two Kalman Filter variants (Extended and Unscented), and three ways of incorporating range measurements. We first use a single range measurement as it is received, and then consider two consecutive range measurements from different CNAs, within the Kalman Filter formulation as a recursive estimator. Finally, we consider relying on the underlying Kalman Filters for dead reckoning between range measurements while incorporating positional corrections using a factor-graph based approach, to include all the range measurements over missions simultaneously in addition to the intermediate Kalman Filter estimates. This integration of a sparse factor graph and Kalman Filter reduces computational load complementing real time execution while maintaining a continuous state estimate. The missions presented in this work are depicted in Fig. 2.

B. Contributions

This work intends to provide several contributions to the field of marine robotics and heterogenous cross-domain autonomy, by:

- First, comparing six filtering techniques across a common dataset, comprising three missions amounting to 3.1 kilometers and 53 minutes of operation, to assess whether they are generalizable.
- Second, quantifying and evaluating trade-offs between using one or multiple CNAs for aiding AUV localization. We also discuss how limited communication bandwidth constrains shared information, leaving out

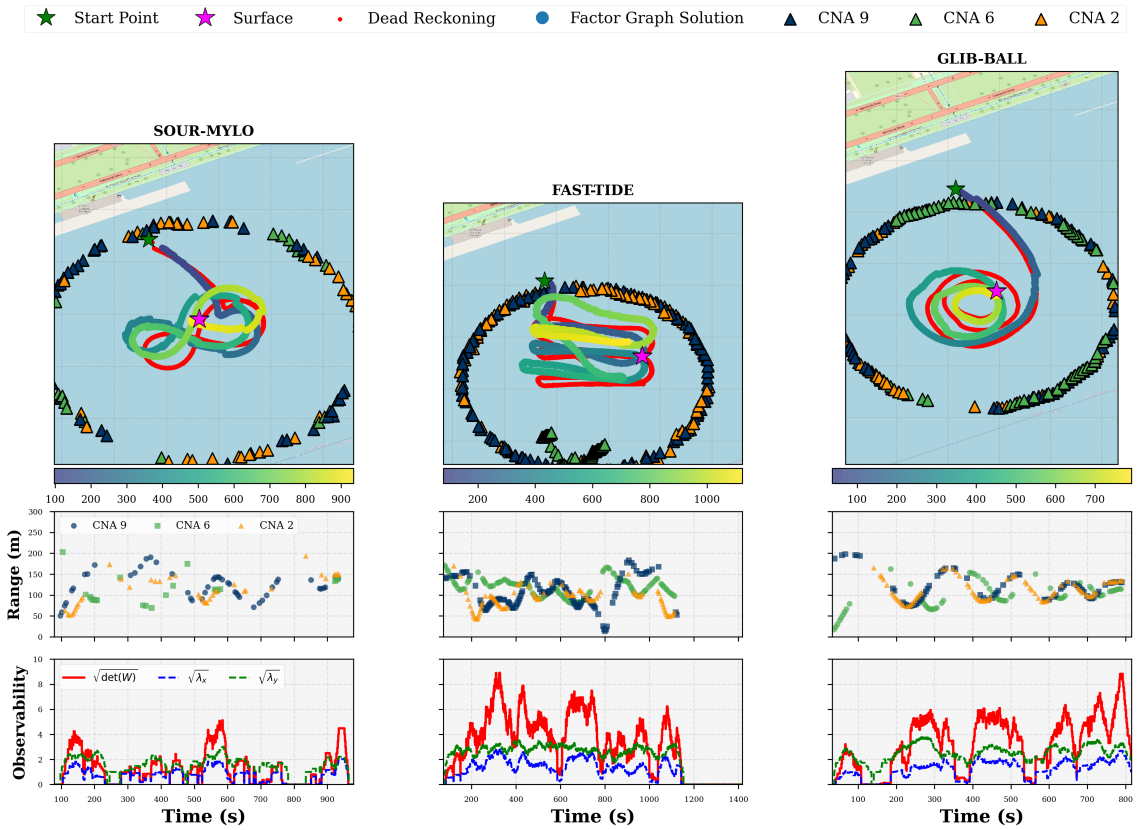

Fig. 2: Trajectory comparison, ranging frequency, and observability metrics for three missions: **SOUR-MYLO** (lemniscate), **FAST-TIDE** (lawnmower), and **GLIB-BALL** (spiral).

unmodeled CNA dynamics. We also show how a single CNA can perform on-par with multiple CNAs if measurements and system dynamics remain temporally observable.

- Third, demonstrating a hybrid Kalman Filter and Factor Graph approach that improves localization accuracy while remaining computationally efficient or on-par with a standard EKF.
- Next, validating a proposed system as a whole, discussing how an MIT Spurdog AUV and low-cost ASVs (such as a BlueBoat), when fitted with the required sensors for this study, may amount to $30,000 (USD, 2025), which sets up future work, by making many-agent systems more realizable.
- Lastly, we achieving comparable results than similar prior work, on more dynamic systems, while demonstrating a viable option when scaling multi-agent systems for underwater navigation, by balancing cost and performance, and opening up future work on closed-loop real time coordination.

II. Related Work

A. General AUV Navigation

Accurate AUV navigation typically relies on dead reckoning and acoustic positioning. Long Baseline (LBL) provides high accuracy by triangulating range measurements from fixed transponders, but it is constrained to predefined areas and requires multiple beacon detections in short succession. Ultra Short Baseline (USBL) systems offer complete tracking by measuring range and bearing from a consolidated acoustic array, eliminating the need for external beacons. However, USBL's accuracy is limited by array size, making it best suited for short-range applications such as docking. While non-acoustic methods exist — such as visual SLAM [1], [2], [3] or terrain-aided navigation [4], these approaches face greater limitations in turbid waters or environments with sparse features. For comprehensive reviews of AUV localization methods, see [5], [6].

B. Moving LBL and Cooperative Navigation

Moving Long Baseline (MLBL) extends traditional LBL by placing transponders on mobile platforms that report both their position and range measurements. Some CNAs incorporate high-accuracy navigation sensors, allowing them to serve as dynamic LBL references. Early MLBL experiments [7] used crewed surface vessels to relay GNSS positions and acoustic ranges to an AUV, but this approach has since evolved into *cooperative navigation*, where multiple platforms share sensor data to improve their state estimates [8], [9]. Unlike MLBL, cooperative navigation removes strict geometric constraints on CNAs, offering greater flexibility in vehicle deployment at the cost of increased communication

and algorithmic complexity [10].

Few public-domain studies have explored ASV-assisted AUV localization at scale. One recent experiment investigated *AUV-assisted diver navigation*, where an AUV provided inter-agent acoustic ranges to inform a diver's state estimate [11]. Using two crewed kayaks equipped with equivalent sensors, the study achieved a 4.5-meter endpoint error while emulating diver motion at 0.5 m/s. Another study used USBL to localize a Graltech X-300 AUV relative to an MGB300 ASV, achieving a 3.94-meter RMS error [12], though both vehicles maintained low relative speeds, at the surface, with a short separation distance and overall mission trajectory, thus simplifying the problem.

The most relevant prior work [13] examined an Iver2 AUV localized relative to an ASV acting as a CNA. The ASV followed a zig-zag trajectory while tracking the AUV, with a Nonlinear Least Squares (NLS) estimator achieving endpoint errors of 15.1 meters and 14.2 meters, later reduced to 11.7 meters and 5.7 meters in post-processing, with a smoothed result which would have been unattainable online. Higher errors were attributed to increased platform speed (1.38 m/s vs. 0.68 m/s), highlighting the difficulty of cooperative navigation in dynamic environments.

III. Methods

A. Overview

Our state estimation framework starts with a traditional Kalman Filter, which is extended to incorporate nonlinear processes and measurement models. We explore both an Extended Kalman Filter (EKF) and an Unscented Kalman Filter (UKF), leveraging three different means of incorporating ranging measurements. Regardless of the range measurement model, the underlying Kalman Filter is used to fuse AHRS, DVL, and pressure sensor measurements for dead reckoning between acoustic ranging measurements. The range measurement models consist of a single range update model, a two range triangulation-based model, and a hybrid approach using both the Kalman Filters and a Factor Graph to optimize applicability in real world scenarios. The latter method incorporates an arbitrary number of range measurements using a factor graph, which is then solved to produce a state estimate that can be used to update the Kalman Filter. This last approach incorporates the complete history of range measurements which is relatively sparse compared to other measurements, to inform the current position estimate.

B. Process and Measurement Models

Here we outline the nonlinear process and measurement models used in the Kalman Filter variants. We first define the AUV states, common to each filter.

$$q = \begin{bmatrix} x & y & z & u & v & w & \psi & \psi_b \end{bmatrix}^T \tag{1}$$

Where we work with a subset of the AUV states - the position in 3D space (x,y,z), the body fixed velocities surge, sway, and heave (u, v, w), and the heading ψ, and the heading bias ψ_b. We exclude roll and pitch from the filter since they are accurately reported by the AHRS and can be used directly.

We then define a discrete time process and measurement model.

$$q_t = f(q_{t-1}, u_{t-1}) + w_{t-1}, \quad w_t \sim \mathcal{N}(0, Q_t) \tag{2}$$

$$z_t = h(q_t) + v_t, \quad v_t \sim \mathcal{N}(0, R_t) \tag{3}$$

We assume all unmodeled dynamics to become normally distributed process noise, w_t, with covariance from a zero-mean of Q_t. We make similar assumptions for the measurement model, such that a measurement z_t may be corrupted with normally distributed measurement noise v_t with a covariance of R_t, where errors are nominally zero-centered.

Subsequently, the process model for this selection of states is assumed to be:

$$f(q_t, u_t) = \begin{bmatrix} x + v_x(q_t)\Delta t \\ y + v_y(q_t)\Delta t \\ z + v_z(q_t)\Delta t \\ u \\ v \\ w \\ \psi + \omega_z \Delta t \\ \psi_b \end{bmatrix} \tag{4}$$

$$\mathbf{v} = \begin{bmatrix} v_x \\ v_y \\ v_z \end{bmatrix} = \mathbf{R}_{NED} \begin{bmatrix} u \\ v \\ w \end{bmatrix} \tag{5}$$

$$\mathbf{R}_{NED} = \mathbf{R}_z(\psi)\mathbf{R}_y(\theta)\mathbf{R}_x(\phi) \tag{6}$$

Where v_x, v_y, and v_z are the velocity components in the global frame, and depend on the vehicle's attitude for roll ϕ, pitch θ, and heading ψ. w_z is the AHRS gyroscope reading for the rotational rate about the z axis in the world frame.

Odometry measurements are obtained from the AHRS (heading), the DVL, and the Bar30 pressure sensor (depth). For these measurements with high confidence, the measurement models are as follows:

$$z_{\text{heading}} = \psi + \psi_b \tag{7}$$

$$z_{\text{depth}} = z \tag{8}$$

$$z_{\text{DVL}} = \begin{bmatrix} u & v & w \end{bmatrix}^T \tag{9}$$

A heading bias is included since these experiments did not use the onboard magnetometer. For the planned mission duration, the heading error induced by noisy magnetometer readings was anticipated to exceed that of the gyroscope drift rate (1.5°/hr). Finally, we measure the depth, z, directly from the Bar30 pressure sensor, and the body fixed velocities with the Tracker 650 DVL.

To incorporate range measurements, we use the spherical measurement model between the reported beacon (ASV)

position (x_b, y_b, z_b), and the AUVs current position estimate ($\hat{x}$, $\hat{y}$, $\hat{z}$). The acoustic transducer was suspended at a known depth of 0.86 meters (34 inches) below each ASV, and z_b is roughly constant provided our operational conditions.

$$z_{\text{range},i} = \sqrt{(x_\text{b} - \hat{x})^2 + (y_\text{b} - \hat{y})^2 + (z_\text{b} - \hat{z})^2}$$

Since depth is measured directly, this measurement model only provides an estimate bounded to the edge of a circle formed by the intersection by the X-Y plane at depth z and the spherical measurement model. For which, there are an infinite many satisfying solutions along the edge of this circle.

To mitigate this ambiguity, we evaluated an alternative measurement model which incorporates two sequential range measurements from different anchors (z_i and z_{i-1}). These measurements are handled simultaneously, constraining the AUV estimated position to one of two possible solutions.

However, this two-range measurement model is only feasible under specific assumptions. Our acoustic communication framework processes a range measurement upper bounded by every 2 seconds. Due to uncertainty in which two measurements are selected for inclusion in this model, the underlying measurements may occur up to 4 seconds apart. This may incur up to a 4 meter difference in the AUV's state. As such, there is increased uncertainty and additional challenges for properly incorporating three measurements sampled across three different AUV states over the period to sample the three CNAs, without including workarounds within the Kalman Filter framework. This then motivates the introduction of the factor graph based approach which best handles these measurements temporally, using sequential single range measurements.

The implications of these measurement models for the linearized EKF are illustrated in Fig. 3, where we take the known CNA position (a beacon), the real position of the AUV, and an incorrect current state estimate $(\hat{x}, \hat{y})$, and illustrate how corrections would be applied in the vector field. In the left plot for the single range measurement model, we can see the case where the measurement is corrected towards a worse estimate, but a satisfying solution. Conversely, we can see that with two range measurements, we constrain the estimate to two satisfying solutions. On multiple CNAs, or a single moving CNA, these issues are typically resolved temporally with consecutive and diverse measurements.

C. Kalman Filters (EKF and UKF)

In this work, we emphasize a hybrid approach for incorporating measurements: by using only a Kalman Filter for full state estimation, or by using a Kalman Filter for intermediate dead reckoning between acoustic measurements, serving as a between factor while updating the position estimate with a factor graph to incorporate the full history of acoustic measurements. This mitigates the need for workarounds in a Kalman Filter based approach. We test both an EKF and

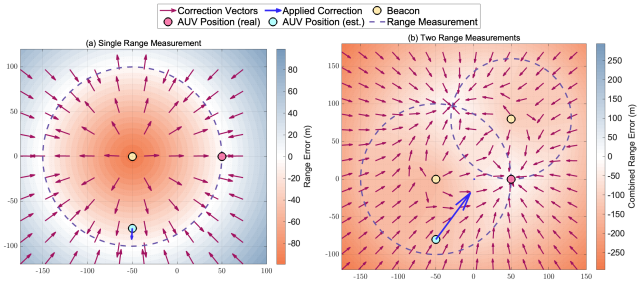

Fig. 3: EKF linearized measurement model: (Left) Single range update may result in suboptimal correction; (Right) Two range updates constrain the solution to two possible estimates, improving accuracy.

the UKF, and compare their performance as a complete estimator, and the boosted performance when combined with a factor graph. For an in-depth discussion on specifically EKFs and UKFs, please refer to [14] and [15] respectively. A standard procedure is applied to the process and measurement models provided in the previous section.

D. Factor Graph

Formulating this process as a NLS optimization problem allows us to include multiple range measurements without the condition that these measurements be near-simultaneous. We seek to solve for the set of AUV states that best satisfy the odometry and all range measurements observed. This consists of constructing a factor graph representing the AUV's trajectory through a set of poses linked by relative pose measurement factors and linked to external references (ASV positions) through range factors. To minimize the computational cost of such a method, the graph is formulated in two dimensions (the horizontal plane) with each AUV state represented by the state variable $x_i \in SE(2)$ and each ASV position represented by variable $l_i \in SO(2)$. $SE(n)$ and $SO(n)$ define special Euclidean and special Orthogonal groups of dimension n.

Furthermore, new pose variables are only created with each new range measurements, resulting in relative small graphs which can be solved quickly by a batch solver.

Relative pose measurements are computed by comparing the state estimate of a Kalman Filter incorporating solely AHRS, DVL, and pressure measurements at two given times. By sampling the state variables x_{i-1} and x_i as well the associated covariances we can obtain the relative pose measurement model,

$$h_{\text{odom}}(x_{i-1}, x_i) \triangleq \ominus x_{i-1} \oplus x_i \tag{10}$$

Likewise we formulate the range measurement model between the AUV and ASV as,

$$h_{\text{range}}(x_i, l_j) \triangleq ||t_{x_i} - t_{l_j}||_2 \tag{11}$$

with an additional prior on the landmark position which accounts for uncertainty in the reported ASV position.

This yields the cost function which can be solved to obtain the set of AUV and ASV states $X \triangleq \{x_i, l_j\}$ which

best satisfy the set of observed measurements: the relative pose obtained from the KF ($z_{\text{odom},i}$), the range measurement ($\hat{z}_{\text{range},j}$), and the reported ASV position ($z_{\text{GPS},j}$).

$$
\begin{aligned}
c(X) = &\sum_i \|h_{\text{odom}}(x_{i-1}, x_i) - z_{\text{odom},i}\|^2_{\Sigma_{\text{odom},i}} \\
&+ \sum_j \|h_{\text{range}}(x_i, l_j) - z_{\text{range},j}\|^2_{\Sigma_{\text{range},j}} \\
&+ \sum_j \|l_j - z_{\text{GPS},j}\|^2_{\Sigma_{\text{GPS},j}} \qquad (12)
\end{aligned}
$$

Finally, the most recent pose in the set is used to update the x, y and ψ components of the the Kalman Filter, leaving the remaining terms unaffected. The marginal covariance of this pose is similarly used to update the associated components of the Kalman Filter covariance.

In practice, this is achieved through by a four step process each time a range measurement is obtained.

1) The KF is sampled to obtain the relative pose measurement and initialize the new AUV state variable.
2) The relative pose factor and range factor are added to the graph, as well as the new AUV and ASV state variables.
3) The graph is solved using a Levenberg-Marquardt solver and the most recent AUV pose-marginal covariance pair is extracted.
4) The extracted pose and covariance are used to update the Kalman Filter.

The underlying factor graph architecture and optimization process is implemented using GTSAM [16], with the underlying Kalman Filter providing continuous state updates between the application of these factor graph-derived corrections. We relax the process noise of the Kalman Filter while increasing our trust in our range measurements, improving both final estimates and the overall trajectory quality, without introducing noise or discontinuities which were obtained with the Kalman Filter with similar parameters.

IV. Experimental Setup

A. Platforms and Operations

For these experiments, we used one modified MIT Spurdog AUV [17] and three Clearpath Heron M302 ASVs, as shown in Fig. 4. The MIT Spurdog AUV was modified with an Ahoi Acoustic Modem [18] and a 3DM-CV7-AHRS from HBK integrated into the payload region (see Fig. 6 of [17], and a Tracker 650 DVL was fitted into an alternative nosecone payload. When the DVL was independently validated against GPS on an ASV, a 4.5% odometry error was observed, where we measured a 1.94 km GPS-referenced odometry, compared to 1.83 km from DVL integration. The total cost of the sensors used in this work is detailed in Table I, providing a breakdown of components necessary for integration into other platforms.

The three Herons were provided a prescribed circular pattern to loiter, while two operators would deploy the Spurdog within the circle to dead-reckon a variety of preset patterns with the DVL and AHRS only during operation. The Spurdog would capture the GPS fix which initialized the dead reckoning solution, and then conduct a continuous operation at roughly 1 m/s and 1 meter of depth before surfacing, and waiting one minute to capture a GPS fix before ending the mission. The autonomy and "guidance system", and all real time software was implemented and is executed within the MOOS-IvP framework [19]. The speed of sound in water was extrapolated with several casts of the RBR*concerto*[3] around the Charles River, where the water temperature was 11 °C, and an estimated speed of sound of 1454 m/s.

Fig. 4: Platforms used for field experiments: (left) an MIT Spurdog AUV, (right) a Clearpath Heron ASV.

TABLE I: Core Sensor Costs for AUV and ASV Platforms

Component	Quantity	Unit Cost (USD)
AUV Hardware		
GPS (Neo-M9N)	1	70
Attitude (HBK 3DM-CV7-AHRS)	1	650
DVL (Tracker 650)	1	2300
ASV Hardware (Per ASV)		
GPS (EVK-M8)	3	200
Attitude (HBK 3DM-CV5-AHRS)	3	650
Shared Acoustic System		
Modem (Ahoi)	4	250
Transducer (AS-1 Hydrophone)	4	410
Total Cost	–	**10,510**

B. Event handling

The operational algorithm is in part illustrated by Fig. 5, with a single CNA for one round. An AUV interrogates the three CNAs in order, making up to two attempts, before moving onto the next CNA. Using low-cost hardware, it is of interest to utilize a TWTT acoustic ranging cycle. With both systems moving simultaneously at 1 m/s in our experiments, the maximum relative velocity is up to 2 m/s, and a maximum measured range of up to 250 meters, as illustrated in Fig. 2. Overall, this provides a maximum TWTT ranging error of 0.7 meters alone.

V. Results

A. Metrics

Filters were tuned to achieve optimal qualitative and quantitative metrics. Qualitatively, we want a solution which is stable, to prevent large discontinuities in a trajectory, so a navigation solution can be used online. In filter tuning, this results in relaxing the measurement uncertainty for

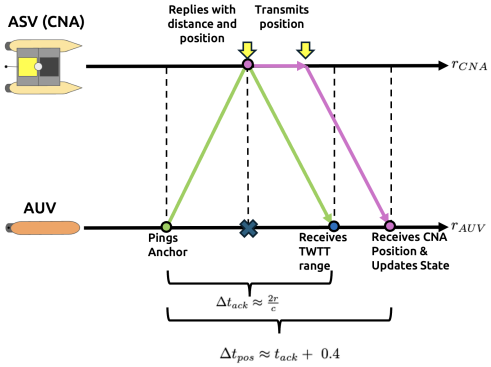

Fig. 5: Two-Way-Travel-Time (TWTT) acoustic communication protocol between AUV and ASV: the AUV initiates ranging, the ASV acknowledges and transmits its GNSS position, enabling range and position estimation.

ranging measurements, such that proportional to the process noise, measurements are incorporated more gradually. This is roughly illustrated in Fig. 3, by the "scale" of the blue vector off of the estimate. Quantitatively, we discuss the Surface Error, and results concerning the range measurements for the last 20% of acoustic measurements, which we refer to as the F20% range mean error (innovation) and RMS Error, and an execution ratio.

1) Surface Error: Quantitatively, our only "ground truth" reference throughout a trajectory is when the AUV surfaces. The surface error, is the absolute measured distance between the reported GNSS position after converting to local meters via a WGS84 geodesic conversion. Ideally, this value is zero. The MIT Spurdog AUV's multi-frequency GNSS receiver and mast is estimated to have a radial error typically to 2-3 meters at the 95% confidence interval, approximated with approaches discussed in [20]. The reported GPS position was consistently measured an average HDOP of 0.64.

2) F20% Mean and RMS Errors: This is the Mean and RMS acoustic-range error between the position estimate and the measurement, over the final 20% of received range measurements. It reflects how the filter converged, assuming the unmodeled dynamics can be characterized by Gaussian noise with a zero centered mean error. The mean error is to capture this metric, while the RMS error is to capture overall noise along this region.

3) Execution Ratio: We record the total time spent running the filter (in post-processing) and divide by the actual mission duration, yielding a ratio in milliseconds-per-second (ms/s). Low ratios indicate feasibility for real time computation on embedded hardware such as the MIT Spurdog AUV's Raspberry Pi 4. The reported numerator, for post-processing duration for a mission, replaying the data as if it was executed in real time, was conducted on a 2021 Apple MacBook M1 Pro. Further, the post-processing analysis was implemented in Python 3, whereas on the AUV it would be implemented in C++, where we would expect significantly improved performance.

4) Dead Reckoning Reference: As a reference, we also report the AUV's dead reckoned navigation solution which was run in real time, which is open-loop with respect to the acoustic ranges, and report the same metrics.

B. Final Results

We provide tabulated results in Table II, which illustrate the metrics discussed in the previous section, applied to the missions depicted in Fig. 2. In Table III, we present the final best results with these filters applied to the three missions. In Fig. 2, we present the dead reckoning solution, which is the *intention* for a prescribed trajectory, compared to the final smoothed factor graph estimate of the total trajectory, which incorporates the final GPS position as a final factor. Because of this, we exclude this final value from the discussion on results since it is unattainable in real time, however it illustrates the most likely trajectory the AUV had taken over the entire mission. Figure 6 illustrates the trajectories of all the filters solely applied to the lemniscate pattern to inform the reader on the qualitative performance of the filters. In the following tables, we prefix a filter and measurement model for single and double ranging measurement models with "S." and "D." respectively, and D.R. for dead reckoning, and F.G. for a factor graph boosted approach.

TABLE II: Tabulated filter mean performance across the three missions depicted in Fig. 2

Filter	Surf. Err. (m)	RMS Err. (m)	Mean Err. (m)	Exec. Ratio (ms/s)
D.R.	19.7	13.8	12.5	N/A
All CNAs [2,6,9]				
S. EKF	9.6	5.4	2.8	7.0
S. UKF	9.3	5.3	2.7	8.7
S. EKF+FG	9.3	3.8	1.8	8.2
S. UKF+FG	9.4	3.4	1.5	10.2
D. EKF	9.0	4.8	1.6	6.9
D. UKF	9.0	4.8	1.7	8.9
Only CNA 2				
S. EKF	10.6	3.4	3.0	6.6
S. UKF	10.1	3.2	2.7	8.4
S. EKF+FG	9.2	1.8	1.3	6.7
S. UKF+FG	9.0	**1.1**	**0.7**	8.7
Only CNA 6				
S. EKF	20.8	3.1	2.4	6.5
S. UKF	20.8	3.0	2.3	8.7
S. EKF+FG	21.1	1.7	1.2	7.0
S. UKF+FG	19.3	1.7	1.2	8.8
Only CNA 9				
S. EKF	11.5	4.5	3.7	**6.4**
S. UKF	10.9	4.4	3.6	8.6
S. EKF+FG	10.0	2.5	1.8	6.8
S. UKF+FG	**8.9**	2.3	1.7	8.7

C. Discussion of Results

Key findings of these results illustrate the viability of the algorithms combined with low-cost sensors, while demonstrating performance on par or better than prior work referenced herein. Using three simultaneous CNAs rendered a more consistent solution on average, however comparable

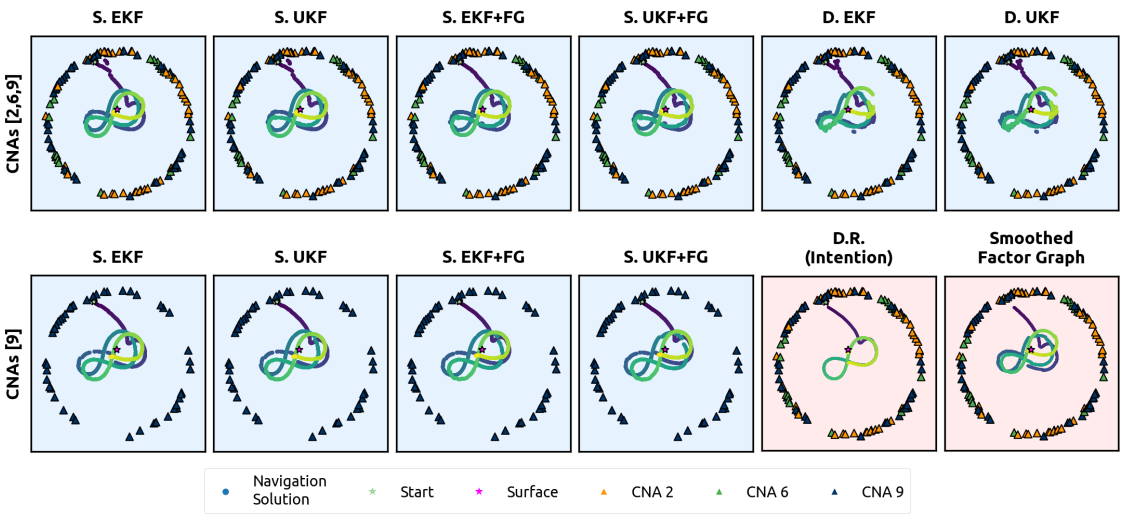

Fig. 6: Comparison of filter performance on the lemniscate mission, **SOUR-MYLO**. Blue groups illustrate proposed filters in this paper, to be ran in real time, while the red groups represent the dead reckoning result (what the AUV thought it was doing), and then the final smoothed factor graph solution including the surfacing position (what the AUV most likely did).

TABLE III: Performance comparison for "in situ" S. UKF+FG with individual CNAs across all missions.

Mission	Surf. Err. (m)	RMS Err. (m)	Mean Err. (m)	Exec. Ratio (ms/s)
Dead Reckoning				
S-M	24.1	17.3	16.5	-
F-T	28.0	17.7	15.6	-
G-B	7.0	6.3	5.3	-
CNAs [2,6,9]				
S-M	4.6	2.9	2.3	9.0
F-T	15.6	5.1	-2.2	11.1
G-B	8.0	2.2	0.0	10.5
CNA 2				
S-M	10.5	0.4	**0.4**	8.7
F-T	7.9	1.5	0.6	8.8
G-B	8.6	1.4	1.2	8.7
CNA 6				
S-M	**3.0**	2.6	2.6	8.5
F-T	40.8	2.3	-0.8	9.3
G-B	14.3	**0.2**	**-0.1**	8.6
CNA 9				
S-M	12.1	1.8	1.4	8.7
F-T	2.3	3.1	1.9	8.9
G-B	12.3	1.9	1.7	8.7

results were achieved with a single CNA. When the reader observes Table III, results were more widely varying for a single agent, especially when only CNA 6 is considered for FAST-TIDE. In this mission, the Heron disconnected from the shoreside network and behaved unexpectedly, thus forming the 'V' shape in FAST-TIDE. Because of this, with the relative position between the ASV and the AUV lacked diversity and AUVs estimate in the X-direction was poorly observed. In our analysis, the sliding window Observability Gramian becomes singular for the associated X eigenvalue, and the AUV's position estimate proceeded to drifted West. Conversely, single CNA 6 was able to achieve essentially performance equal to the three simultaneous CNAs, by maintaining rich enough relative positions to the AUV throughout the mission, which is illustrated in the blue subplots at the bottom of Fig. 6.

Next, in our model since we are bandwidth constrained via acoustic communication, we assume that the CNA's position estimate is a "ground truth" reference, which is not strictly correct. The CNA's position has unmodeled behavior which was not transmitted to the AUV due to bandwidth constraints, which in all, introduces more uncertainty into the system. This result is demonstrated by the lower F20% RMS and range mean errors found in Table II, where the AUV is more closely coupled to a single CNA, rather than three simultaneously. When three CNAs are considered, the algorithm finds an equilibrium between three different systems with unmodeled dynamics. The factor graph-based methods can more simply account for this by incorporating a loose prior on the CNA position, allowing some deviation from the initial value which partially accounts for these unmodeled aspects.

This raises the discussion on a few key points:

- An accurate estimate can be achieved with a single CNA, *without* adaptive positioning, which may further optimize positioning and measurement quality relative to the AUV. Therefore, this motivates future work in closed-loop adaptive CNA positioning with this work.
- If an accurate estimate can be achieved with a single CNA, it becomes more viable to share more information between the AUV and CNA to improve estimation through more closely coupled models.
- Not only is the combined filter's performance a top performer, it is also feasible to run in real time on the AUV and embedded hardware, such as the Raspberry Pi 4 on the MIT Spurdog AUV.

VI. Conclusions & Future Work

This paper presents a comprehensive evaluation of cooperative localization techniques for a low-cost AUV, the MIT Spurdog, where ASVs serve as Communication/Navigation Aids by providing an acoustic range measurement and their positional estimate. We compared six different combinations of filtering techniques across three field trials, totaling 53 minutes of operation and 3.1 kilometers of data. Our best results were achieved using a hybrid approach combining an Unscented Kalman Filter with a Factor Graph, using single range measurements (S. UKF+FG). Results were more consistent when multiple CNAs are employed simultaneously, however comparable results were achieved with a single CNA despite the lack of adaptive real time coordination. For three simultaneous CNAs, we achieved an average final surfacing error of 9.0 meters, an F20% Range Mean Error of 0.7 meters, and an F20% RMS error of 1.1 meters. Excluding the mission where acoustic ranges were unavailable for the final 200 seconds for the mission, the average surface error was 6.3 meters.

We isolate and apply the top-performing algorithm to each CNA alone to demonstrate differences in performance due to the variability in the CNA's and AUV's relative trajectory. Our approach's execution ratio of 9.5 ms/s, demonstrates the likely feasibility for real time implementation on embedded hardware such as the Raspberry Pi 4 used in the MIT Spurdog AUV. Overall, the results demonstrate that low-cost platforms and sensors can achieve navigation performance comparable to or better than prior work which has used more expensive and sophisticated systems. This has significant implications for enabling large-scale, multi-agent operations in marine environments where cost and scalability are important considerations.

From these results, and what motivated this study, is based on future work:

- Implementing closed-loop heterogeneous coordination where ASVs adaptively position themselves to optimize measurement quality and observability.
- Since the results were evaluated in post processing, when two CNAs were stripped away the time between ranging measurements were at least tripled. With this observation, communication bandwidth can be allocated where an AUV and CNA can share more information for real time coordination and improved estimation.
- Leveraging the sliding window Observability Gramian as a metric to inform CNA behaviors to provide high-quality measurements to the AUV in operation.

This work is a step towards further enabling closed-loop heterogeneous marine robotic teams where low-cost AUVs can maintain accurate navigation through cooperation with ASVs, enabling wider range of scientific, commercial, and defense applications.

Acknowledgements

The authors would like to thank Jeremy Wenger, Filip Strømstad, Tyler Paine, and Jungseok Hong for supporting preliminary field tests and operations.

References

[1] D. A. Duecker, N. Bauschmann, T. Hansen, E. Kreuzer, and R. Seifried, "Towards micro robot hydrobatics: Vision-based guidance, navigation, and control for agile underwater vehicles in confined environments," in *IEEE International Conference on Intelligent Robots and Systems (IROS)*, (Las Vegas, NV, USA), pp. 1819–1826, IEEE, 2020.

[2] R. M. Eustice, O. Pizarro, and H. Singh, "Visually augmented navigation for autonomous underwater vehicles," *IEEE Journal of Oceanic Engineering*, vol. 33, no. 2, pp. 103–122, 2008.

[3] L. Zhao, M. Zhou, and B. Loose, "Tightly-coupled visual-dvl-inertial odometry for robot-based ice-water boundary exploration," in *2023 IEEE/RSJ International Conference on Intelligent Robots and Systems (IROS)*, pp. 7127–7134, IEEE, 2023.

[4] G. T. Donovan, "Position error correction for an autonomous underwater vehicle inertial navigation system (ins) using a particle filter," *IEEE Journal of Oceanic Engineering*, vol. 37, no. 3, pp. 431–445, 2012.

[5] L. Paull, S. Saeedi, M. Seto, and H. Li, "Auv navigation and localization: A review," *IEEE Journal of Oceanic Engineering*, vol. 39, no. 1, pp. 131–149, 2014.

[6] S. Watson, D. A. Duecker, and K. Groves, "Localisation of unmanned underwater vehicles (uuvs) in complex and confined environments: A review," *Sensors*, vol. 20, no. 21, p. 6203, 2020.

[7] J. Vaganay, J. Leonard, J. Curcio, and J. Willcox, "Experimental validation of the moving long base-line navigation concept," in *2004 IEEE/OES Autonomous Underwater Vehicles (IEEE Cat. No.04CH37578)*, pp. 59–65, 2004.

[8] A. Bahr, J. J. Leonard, and M. F. Fallon, "Cooperative localization for autonomous underwater vehicles," *The International Journal of Robotics Research*, vol. 28, no. 6, pp. 714–728, 2009.

[9] S. E. Webster, J. M. Walls, L. L. Whitcomb, and R. M. Eustice, "Decentralized extended information filter for single-beacon cooperative acoustic navigation: Theory and experiments," *IEEE Transactions on Robotics*, vol. 29, no. 4, pp. 957–974, 2013.

[10] M. F. Fallon, G. Papadopoulos, and J. J. Leonard, "A measurement distribution framework for cooperative navigation using multiple auvs," in *2010 IEEE International Conference on Robotics and Automation*, pp. 4256–4263, 2010.

[11] J. R. Pelletier, B. W. O'Neill, J. J. Leonard, L. Freitag, and E. Gallimore, "Auv-assisted diver navigation," *IEEE Robotics and Automation Letters*, vol. 7, no. 4, pp. 10208–10215, 2022.

[12] M. Bresciani, G. Peralta, F. Ruscio, L. Bazzarello, A. Caiti, and R. Costanzi, "Cooperative asv/auv system exploiting active acoustic localization," in *2021 IEEE/RSJ International Conference on Intelligent Robots and Systems (IROS)*, pp. 4337–4342, IEEE, 2021.

[13] M. F. Fallon, G. Papadopoulos, J. J. Leonard, and N. M. Patrikalakis, "Cooperative auv navigation using a single maneuvering surface craft," *The International Journal of Robotics Research*, vol. 29, no. 12, pp. 1461–1474, 2010.

[14] A. H. Jazwinski, *Stochastic Processes and Filtering Theory*, vol. 64 of *Mathematics in Science and Engineering*. San Diego, CA: Academic Press, 1970.

[15] E. A. Wan and R. Van Der Merwe, "The unscented kalman filter for nonlinear estimation," in *Proceedings of the IEEE 2000 adaptive systems for signal processing, communications, and control symposium (Cat. No. 00EX373)*, pp. 153–158, Ieee, 2000.

[16] F. Dellaert and G. Contributors, "borglab/gtsam," May 2022.

[17] R. Turrisi, H. Huang, F. Stromstad, J. Morrison, A. Papalia, J. Leonard, and M. Benjamin, "The spurdog auv: A field configurable and optionally a-sized low-cost auv," in *2024 IEEE/OES Autonomous Underwater Vehicles Symposium (AUV)*, (Boston, MA, USA), October 2024.

[18] B.-C. Renner, J. Heitmann, and F. Steinmetz, "ahoi: Inexpensive, low-power communication and localization for underwater sensor networks and μauvs," *ACM Trans. Sen. Netw.*, vol. 16, Jan. 2020.

[19] M. R. Benjamin, H. Schmidt, P. M. Newman, and J. J. Leonard, "Nested autonomy for unmanned marine vehicles with moos-ivp," *Journal of Field Robotics*, vol. 27, no. 6, pp. 834–875, 2010.

[20] E. Kaplan and C. Hegarty, "Understanding gps/gnss: Principles and applications, third edition," 2017.